MEASUREMENT OF MULTIJET CROSS-SECTION RATIOS IN PROTON-PROTON COLLISIONS WITH THE CMS DETECTOR AT THE LHC

A THESIS

Submitted to the

FACULTY OF SCIENCE

PANJAB UNIVERSITY, CHANDIGARH

for the degree of

DOCTOR OF PHILOSOPHY

2017

Anterpreet Kaur

DEPARTMENT OF PHYSICS

CENTRE OF ADVANCED STUDY IN PHYSICS

PANJAB UNIVERSITY, CHANDIGARH

INDIA

Dedicated to

my Grand-Parents

&

Parents

Contents

List of Figures xi

List of Tables xiii

---

1 Measurement of the Differential Inclusive Multijet Cross Sections and their Ratio 1

1.1 Data Samples 2

1.1.1 Monte Carlo Samples 3

1.2 Event Selection 4

1.2.1 Trigger Selection 4

1.2.2 Primary Vertex Selection 6

1.2.3 Missing Transverse Energy Cut 8

1.2.4 Jet Identification 9

1.2.4.1 Jet ID Efficiency 10

1.2.5 Jet Energy Corrections and Selection 13

1.3 Comparison with Simulated Events 14

1.3.1 Pile-up Reweighting 14

1.3.2 Cross Section Comparison 15

List of publications 17

Reprints **19**

List of Figures

1.1 Trigger efficiencies turn-on curves for the single jet trigger paths used in the analysis.To determine the 99% efficiency threshold, the trigger turn-on curves are fitted using a sigmoid function taking into account the uncertainties using Clopper-Pearson confidence intervals. 7

1.2 Missing transverse energy fraction of the total transverse energy per event in data and simulated events in inclusive 2-jet (left) and 3-jet events (right). To remove background and noise, events with a fraction exceeding a certain threshold, here indicated with the red dashed line, are rejected. 9

1.3 The fractions of jet constituents as observed in data and simulated events for different types of PF candidates for inclusive 2-jet events. Data and simulation are normalized to the same number of events. The distributions are shown after the application of the jet ID. 11

1.4 The fractions of jet constituents as observed in data and simulated events for different types of PF candidates for inclusive 3-jet events. Data and simulation are normalized to the same number of events. The distributions are shown after the application of the jet ID. 12

1.5 The jet ID efficiency studied using a tag-and-probe technique on dijet event topologies, is shown as a function of $H_{T,2}/2$ for inclusive 2-jet (left) and 3-jet events (right) and it always exceeds 99%. 13

1.6 Number of reconstructed vertices in data and simulated events before (left) and after (right) the pile-up reweighting. 14

1.7 The differential cross section as a function $H_{T,2}/2$ for inclusive 2-jet events (top left), for inclusive 3-jet events (top right) and for inclusive 4-jet events (bottom), for data (black solid circles), MadGraph5 + pythia6 MC (red solid circles) and NLO (histogram). Ratios between the MC predictions and the data as well as between the NLO predictions and the data are shown in bottom panel of each plot. 16

List of Tables

1.1 Four data sets collected in run periods A, B,C and D during 2012, along with the corresponding run numbers and luminosity. 3

1.2 The official MC production samples generated in phase space slices in H_{T} with the generator MadGraph5 and interfaced to pythia6 for the parton shower and hadronization of the events. The cross section and number of events generated are mentioned for each sample. . . . 4

1.3 List of all single jet trigger paths used in the analysis. The column $\mathrm{H_{T,2}}/2$, 99% indicates the value of $H_{\mathrm{T},2}/2$ at which each trigger exhibits an efficiency larger than 99%. The last column reports the effective luminosity seen by each trigger. This number, divided by the total integrated luminosity of 19.71 fb^{-1}, gives the effective prescale applied on a trigger over the whole run period. 5

1.4 The jet ID removes noise and fake jets based on the properties of the reconstructed jets and the clustered particle candidates. All the selection cuts which are recommended by the JETMET group are applied [1]. 10

Chapter 1

Measurement of the Differential Inclusive Multijet Cross Sections and their Ratio

The inclusive *n-jet* event samples include the events with number of jets $\geq n$, where $n = 2$ and 3 in the current study. The inclusive multijet event yields are transformed into a differential cross section which is defined as :

$$\frac{\mathrm{d}\sigma}{\mathrm{d}\big(H_{\mathrm{T},2}/2\big)} = \frac{1}{\epsilon\ \mathcal{L}_{\mathrm{int,eff}}} \frac{N_{\mathrm{event}}}{\Delta\big(H_{\mathrm{T},2}/2\big)} \tag{1.1}$$

where N_{event} is the number of inclusive 2- or 3-jet events counted in an $H_{\mathrm{T},2}/2$ bin, ϵ is the product of the trigger and jet selection efficiencies, which are greater than 99%, $\mathcal{L}_{\mathrm{int,eff}}$ is the effective integrated luminosity, and $\Delta\big(H_{\mathrm{T},2}/2\big)$ are the bin widths. The measurements are reported in units of (pb/GeV).

The differential inclusive multijet cross sections are measured as a function of the average transverse momentum, $H_{\mathrm{T},2}/2 = \frac{1}{2}(p_{\mathrm{T},1} + p_{\mathrm{T},2})$, where $p_{\mathrm{T},1}$ and $p_{\mathrm{T},2}$ denote the transverse momenta of the two leading jets. The cross section ratio R_{32}, defined in Eq. 1.2 is obtained by dividing the differential cross sections of inclusive

3-jet events to that of inclusive 2-jet one, for each bin in $H_{\mathrm{T},2}/2$.

$$R_{32} = \frac{\frac{\mathrm{d}\sigma_{3\text{-}jet}}{\mathrm{d}\left(H_{\mathrm{T},2}/2\right)}}{\frac{\mathrm{d}\sigma_{2\text{-}jet}}{\mathrm{d}\left(H_{\mathrm{T},2}/2\right)}} \tag{1.2}$$

For inclusive 2-jet events ($\mathrm{n_j} \geq 2$) sufficient data are available up to $H_{\mathrm{T},2}/2 = 2\,\mathrm{TeV}$, while for inclusive 3-jet events ($\mathrm{n_j} \geq 3$) and the ratio R_{32}, the accessible range in $H_{\mathrm{T},2}/2$ is limited to $H_{\mathrm{T},2}/2 < 1.68\,\mathrm{TeV}$.

1.1 Data Samples

This measurement uses the data collected at the center of mass energy of 8 TeV by CMS experiment in the 2012 run period of the LHC. The 2012 data is taken in four periods A, B, C, D and the data sets are divided into samples according to the run period. Further each sample is grouped into subsets based on the trigger decision. For run B-D, the `JetMon` stream datasets contain prescaled low trigger threshold paths (HLTPFJet40, 80, 140, 200 and 260) while the `JetHT` stream datasets contain unprescaled high threshold trigger paths (HLT PFJet320 and 400). For run A, the `Jet` stream contains all the above mentioned trigger paths. The data to be used in physics analysis must satisfy a certain criteria which include proper performance of all detector subsystems as well as the passing of data quality monitoring (DQM) steps during the validation process. CMS uses JSON (Java Script Object Notation) format files to store the range of good lumi sections within a run. In the current analysis, the applied certification file[1] is based on the final event reconstruction of the 2012 CMS data sets. The datasets used in the current study are mentioned in the Table 1.1 along with the luminosity of each dataset.

[1] Cert_190456-208686_8TeV_22Jan2013ReReco_Collisions12_JSON

Table 1.1: Four data sets collected in run periods A, B,C and D during 2012, along with the corresponding run numbers and luminosity.

Run	Run range	Data set	Luminosity fb^{-1}
A	190456-193621	/Jet/Run2012A-22Jan2013-v1/AOD	0.88
B	193834-196531	/Jet[Mon,HT]/Run2012B-22Jan2013-v1/AOD	4.41
C	198022-203742	/Jet[Mon,HT]/Run2012C-22Jan2013-v1/AOD	7.06
D	203777-208686	/Jet[Mon,HT]/Run2012D-22Jan2013-v1/AOD	7.37

The data sets have the LHC luminosity increasing with period, full data sample of 2012 corresponds to an integrated luminosity of 19.71 fb^{-1}.

1.1.1 Monte Carlo Samples

To have a comparison of data results with the simulated events, the MadGraph5 [2] Monte-Carlo event generator has been used. The MadGraph5 generates matrix elements for High Energy Physics processes, such as decays and $2 \to n$ scatterings. The underlying event is modeled using the tune Z2*. It has been interfaced to pythia6 [3] by the LHE event record [4], which generates the rest of the higher-order effects using the Parton Showering (PS) model. Matching algorithms ensure that no double-counting occurs between the tree-level and the PS-model-generated partons. The MC samples are processed through the complete CMS detector simulation to allow studies of the detector response and compare to measured data on detector level.

The cross section measured as a function of the transverse momentum p_{T} or the scalar sum of the transverse momentum of all jets H_{T} falls steeply with the increasing p_{T}. So in the reasonable time, it is not possible to generate a large number of high p_{T} events. Hence, the events are generated in the different phase-space region binned in H_{T} or the leading jet p_{T}. Later on, the different phase-space regions are added together in the data analyses by taking into account the cross section of the different phase-space regions. The official CMS MadGraph5 + pythia6 MC samples used in

this analysis are generated as slices in the H_T phase-space are tabulated in Table 1.2 along with their cross sections and number of events generated.

Table 1.2: The official MC production samples generated in phase space slices in H_T with the generator MadGraph5 and interfaced to pythia6 for the parton shower and hadronization of the events. The cross section and number of events generated are mentioned for each sample.

Generator	Sample	Events	Cross Section pb
MadGraph5 + pythia 6	/QCD_HT-100To250_TuneZ2star_8TeV-madgraph-pythia6/ Summer12_DR53X-PU_S10_START53_V7A-v1/AODSIM	50129518	1.036×10^7
	/QCD_HT-250To500_TuneZ2star_8TeV-madgraph-pythia6/ Summer12_DR53X-PU_S10_START53_V7A-v1/AODSIM	27062078	2.760×10^5
	/QCD_HT-500To1000_TuneZ2star_8TeV-madgraph-pythia6/ Summer12_DR53X-PU_S10_START53_V7A-v1/AODSIM	30599292	8.426×10^3
	/QCD_HT-1000ToInf_TuneZ2star_8TeV-madgraph-pythia6/ Summer12_DR53X-PU_S10_START53_V7A-v1/AODSIM	13843863	2.040×10^2

1.2 Event Selection

To yield a multijet sample with high purity and high selection efficiency, the events are selected according to several quality criteria. This event selection also reduces beam induced background, detector-level noise and jets arising from fake calorimeter energy deposits.

1.2.1 Trigger Selection

CMS implements a trigger system organized in two levels, in order to reduce the amount of recorded events to a sustainable rate. This analysis deals with jets in the final state, so single jet trigger paths are used to select events in data which consists of one L1 trigger seed and multiple HLT filters. The L1 jet trigger uses transverse energy sums computed using both HCAL and ECAL in the central region ($|\eta| < 3.0$) or HF in the forward region ($|\eta| > 3.0$). A more elaborate but still very fast algorithm, the "jet finder", is then implemented on the energy cluster but with a finer segmentation in order to select the raw object for the HLT trigger :

the algorithm makes use of a cone size in order to cluster in a primitive jet the calorimeter towers whose energy is larger than the seed threshold. If the primitive HLT jet has an energy above the threshold set by the trigger, the event is selected and the collection of recorded data is saved and stored in streams. The single jet triggers used for this analysis are tabulated in Table 1.3. HLT_PFJetX implies that there is at-least one jet in the event, whose $p_{\mathrm{T}} > \mathrm{X}$ (GeV). The L1 trigger has a lower threshold to ensure full efficiency versus p_{T} of the HLT trigger. The p_{T} spectrum is steeply falling and hence the rates for low-p_{T} jets are very high. So it is not feasible to use a single unprescaled trigger for the selection of all required events. To collect sufficient data in the lower part of the p_{T} spectrum, different five prescaled low-p_{T} trigger paths, each with different prescale value, are used. Also, one unprescaled trigger i.e. HLT_Jet320 is used in the high p_{T} region, in which the rate is sufficiently small to collect and store all events.

Table 1.3: List of all single jet trigger paths used in the analysis. The column $\mathrm{H_{T,2}}/2$, 99% indicates the value of $H_{\mathrm{T},2}/2$ at which each trigger exhibits an efficiency larger than 99%. The last column reports the effective luminosity seen by each trigger. This number, divided by the total integrated luminosity of 19.71 fb^{-1}, gives the effective prescale applied on a trigger over the whole run period.

Trigger Path	**L1 threshold** GeV	**HLT threshold** GeV	$\boldsymbol{H_{\mathrm{T},2}/2}$**, 99%** GeV	**Eff. Lumi** fb^{-1}
HLT_PFJet80	36	80	120.0	0.21×10^{-2}
HLT_PFJet140	68	140	187.5	0.56×10^{-1}
HLT_PFJet200	92	200	262.5	0.26
HLT_PFJet260	128	260	345.0	1.06
HLT_PFJet320	128	320	405.0	19.71

The efficiency of each trigger, as a function of the measured observable, is described by the turn-on curves with a rising part, where the trigger is partly inefficient, until a plateaux region, corresponding to the region of full efficiency of the trigger. Hence it is necessary to determine the threshold above which a trigger becomes fully efficient. It is defined as the value at which the efficiency exceeds 99%. In the assumption that the reference trigger HLT_PFJetX is fully efficient in the considered region of the phase space, the trigger efficiency for HLT_PFJetY is

defined as Eq. 1.3. The value of X is chosen previous to that of Y in p_{T} ordering from the trigger list so that the higher trigger condition can be emulated from the lower trigger path.

$$\epsilon_{\mathrm{HLT\_PFJetY}} = \frac{H_{\mathrm{T},2}/2\Big(\mathrm{HLT\_PFJetX} + (\mathrm{L1Object\_p_T} > \mathrm{Z}) + (\mathrm{HLTObject\_p_T} > \mathrm{Y})\Big)}{H_{\mathrm{T},2}/2(\mathrm{HLT\_PFJetX})} \tag{1.3}$$

where Y indicates the p_{T} threshold of HLT_PFJetY and Z is the L1 seed value corresponding to the trigger path HLT_PFJetY. The denominator represents the number of events for which the reference trigger path HLT_PFJetX has been fired. The numerator is the number of events for which HLT_PFJetX has been fired along the p_{T} of L1Object $\geq$ Z and the p_{T} of HLTObject $\geq$ Y. For example, in order to obtain turn-on curve for HLT_PFJet260, the reference HLT path HLT_PFJet200 is chosen, the p_{T} cut on L1Object is 128 GeV and p_{T} cut on HLTObject is 260 GeV. The uncertainty on the efficiency is indicated by error bars which represent Clopper-Pearson confidence intervals [5]. To determine the point, at which the trigger efficiency is larger than 99%, the turn-on distribution is fitted using a sigmoid function described in Eq. 1.4. The trigger turn-on curves as a function of $H_{\mathrm{T},2}/2$ can been seen in Fig. 1.1.

$$f_{fit}(x) = \frac{1}{2}\left(1 + erf\left(\frac{x-\mu}{\sqrt{2}\sigma}\right)\right) \tag{1.4}$$

1.2.2 Primary Vertex Selection

A primary vertex (PV) is identified by a collection of tracks, measured in the tracker with a good fit quality between the hits and compatible with the beam line. The tracks are clustered according to the z-coordinate of their point of closest approach

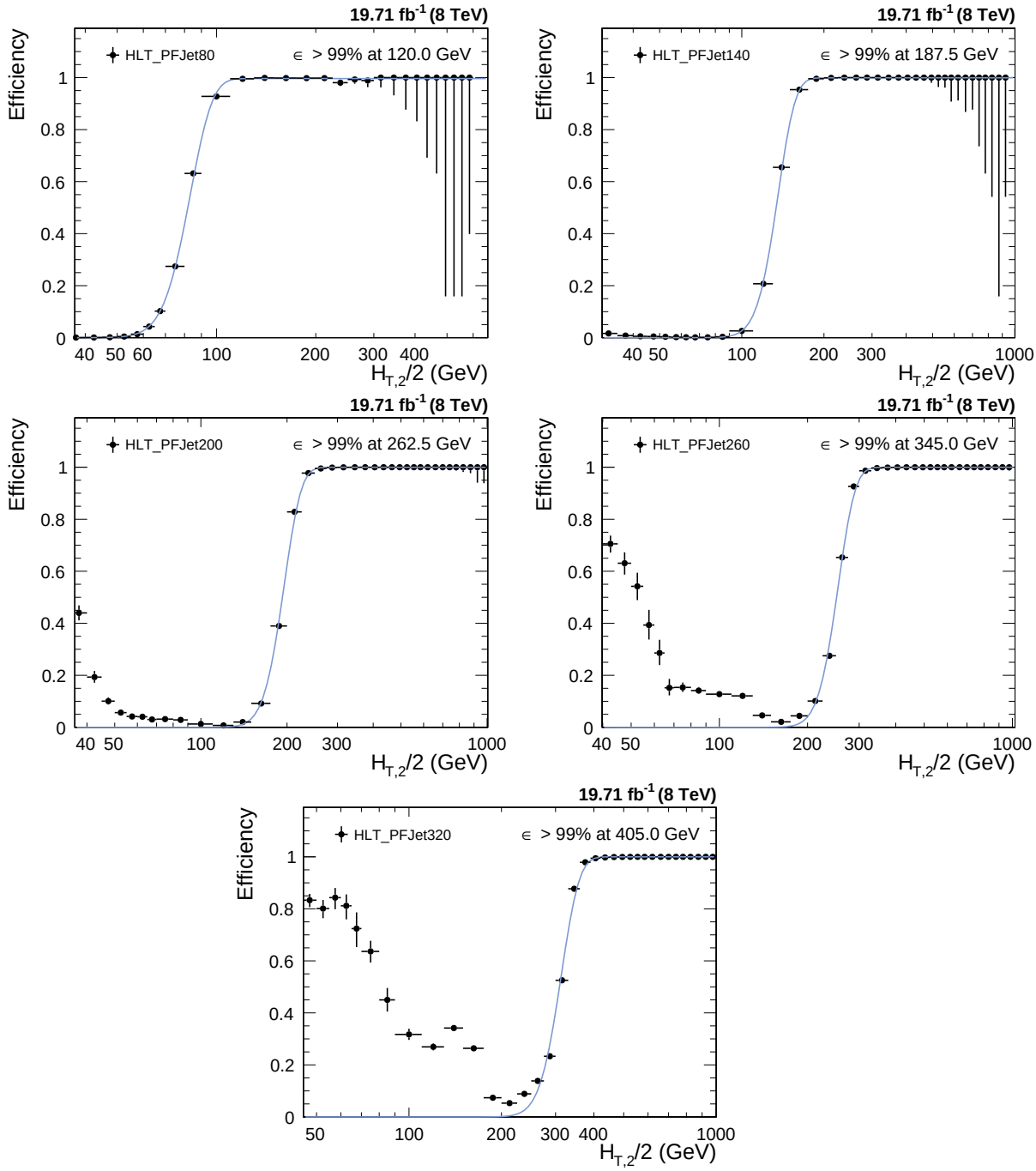

Figure 1.1: Trigger efficiencies turn-on curves for the single jet trigger paths used in the analysis.To determine the 99% efficiency threshold, the trigger turn-on curves are fitted using a sigmoid function taking into account the uncertainties using Clopper-Pearson confidence intervals.

to the beam axis. Each event is required to have at least one good PV which is well reconstructed within a distance of $\left|z(PV)\right| < 24$ cm to the nominal interaction point of the detector. Also the radial distance in x-y plane, ρ(PV) should be smaller than 2 cm. The number of degrees of freedom in vertex fit needs to be at-least four. Thus, at least four tracks must be present in order to perform a valid vertex fit.

1.2.3 Missing Transverse Energy Cut

If all particles could be identified and perfectly measured, the transverse momentum of all particles would sum up to zero. Neutral weakly interacting particles, such as neutrinos, escape from typical collider detectors without producing any direct response in the detector elements. The presence of such particles must be inferred from the imbalance of total momentum of all visible particles. The vector momentum imbalance in the plane perpendicular to the beam direction is known as missing transverse momentum or energy ($E_{\mathrm{T}}^{\mathrm{miss}}$). It is one of the most important observables for discriminating leptonic decays of W bosons and top quarks from background events which do not contain neutrinos, such as multijet and Drell–Yan events or searches for physics beyond the Standard Model which involve undetectable particles.

The ratio of missing transverse energy to the total transverse energy $E_{\mathrm{T}}^{\mathrm{miss}}/\sum E_{\mathrm{T}}$, shown in Fig. 1.2 for $\mathrm{n_j} \geq 2$ (left) and $\mathrm{n_j} \geq 3$ (right), shows a discrepancy between data and MC at the tail part of the distribution. This is because of a finite contribution from $\mathrm{Z}(\rightarrow \nu\bar{\nu})$ + jet events which gives rise to non-zero E_{T} in the events in data. Such events are absent in QCD simulated events in MC. Hence $E_{\mathrm{T}}^{\mathrm{miss}}/\sum E_{\mathrm{T}}$ is required to be less than 0.3 to reject events with high $E_{\mathrm{T}}^{\mathrm{miss}}$.

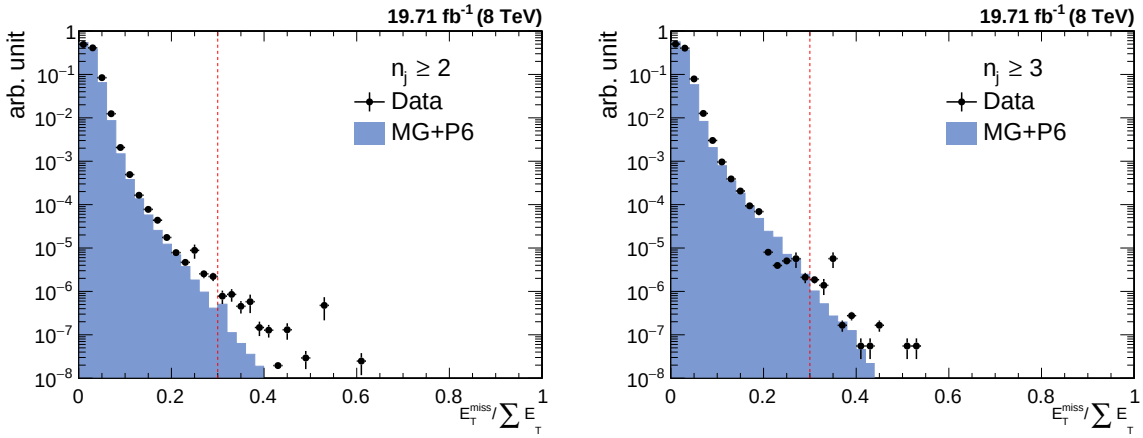

Figure 1.2: Missing transverse energy fraction of the total transverse energy per event in data and simulated events in inclusive 2-jet (left) and 3-jet events (right). To remove background and noise, events with a fraction exceeding a certain threshold, here indicated with the red dashed line, are rejected.

1.2.4 Jet Identification

In order to suppress fake jets, arising from detector noise or misreconstructed particles, jet identification criteria (ID) has been applied. Instead of applying it event-wise, it is applied it on each jet. The algorithm works on reconstructed jets using information of the clustered particle candidates. The official tight jet ID [6], recommended by JETMET group [1] is used. Due to pileup and electronic noise the jet constituent fractions may vary from event to event. In order to reject the noisy jets, some jet selection criteria are optimized to select only good quality jets. The selection criteria are implemented as selection cut on jet fractions. Table 1.4 summarizes the properties of the reconstructed jets and their respective cuts. Each jet should contain at least two particles, one of which should be a charged hadron. The cut on the fraction of neutral hadrons and photons removes HCAL noise and ECAL noise, respectively. Muons that are falsely identified and clustered as jets are removed by the muon fraction criterion. Based on information of the tracker, additional selection cuts are enforced in the region $|\eta| < 2.4$. The charged electromagnetic fraction cut removes the jets clustered from misidentified electrons. Furthermore, the fraction of charged hadrons in the jet must be larger than zero and jets without any charged hadrons are very likely to be pileup jets. The Figures 1.3 and 1.4 show

the distributions of the jet constituents observed in data and simulated events for $n_j \geq 2$ and $n_j \geq 3$, respectively.

Table 1.4: The jet ID removes noise and fake jets based on the properties of the reconstructed jets and the clustered particle candidates. All the selection cuts which are recommended by the JETMET group are applied [1].

	Property	**Loose ID**	**Tight ID**
Whole η region	neutral hadron fraction	< 0.99	< 0.90
	neutral EM fraction	< 0.99	< 0.90
	number of constituents	> 1	> 1
	muon fraction	< 0.80	< 0.80
only $\|\eta\| < 2.4$	charged hadron fraction	> 0	> 0
	charged multiplicity	> 0	> 0
	charged EM fraction	< 0.99	< 0.90

1.2.4.1 Jet ID Efficiency

The efficiency of the jet ID as a function of $H_{T,2}/2$ is studied using a tag-and-probe technique with dijet events. The two leading jets are required to be back-to-back in the azimuthal plane such that $|\Delta\phi - \pi| < 0.3$. One of the dijets is selected randomly as a "tag" jet which is required to fulfill the tight jet ID criteria. The other jet is called "probe" jet for which it is examined, whether it also passes the tight jet ID. The ID efficiency is defined as the ratio of events where the probe jet passes the ID requirements, over the total number of dijet events. Figure 1.5 shows the ID efficiency as a function of $H_{T,2}/2$ for $n_j \geq 2$ (left) and $n_j \geq 3$ (right) ?. As expected, the jet ID efficiency is larger than 99%. The QCD cross section decreases as a function of $H_{T,2}/2$ and hence the number of events decrease on moving to higher $H_{T,2}/2$. Consequently the statistical fluctuations for ID efficiency are larger at higher $H_{T,2}/2$.

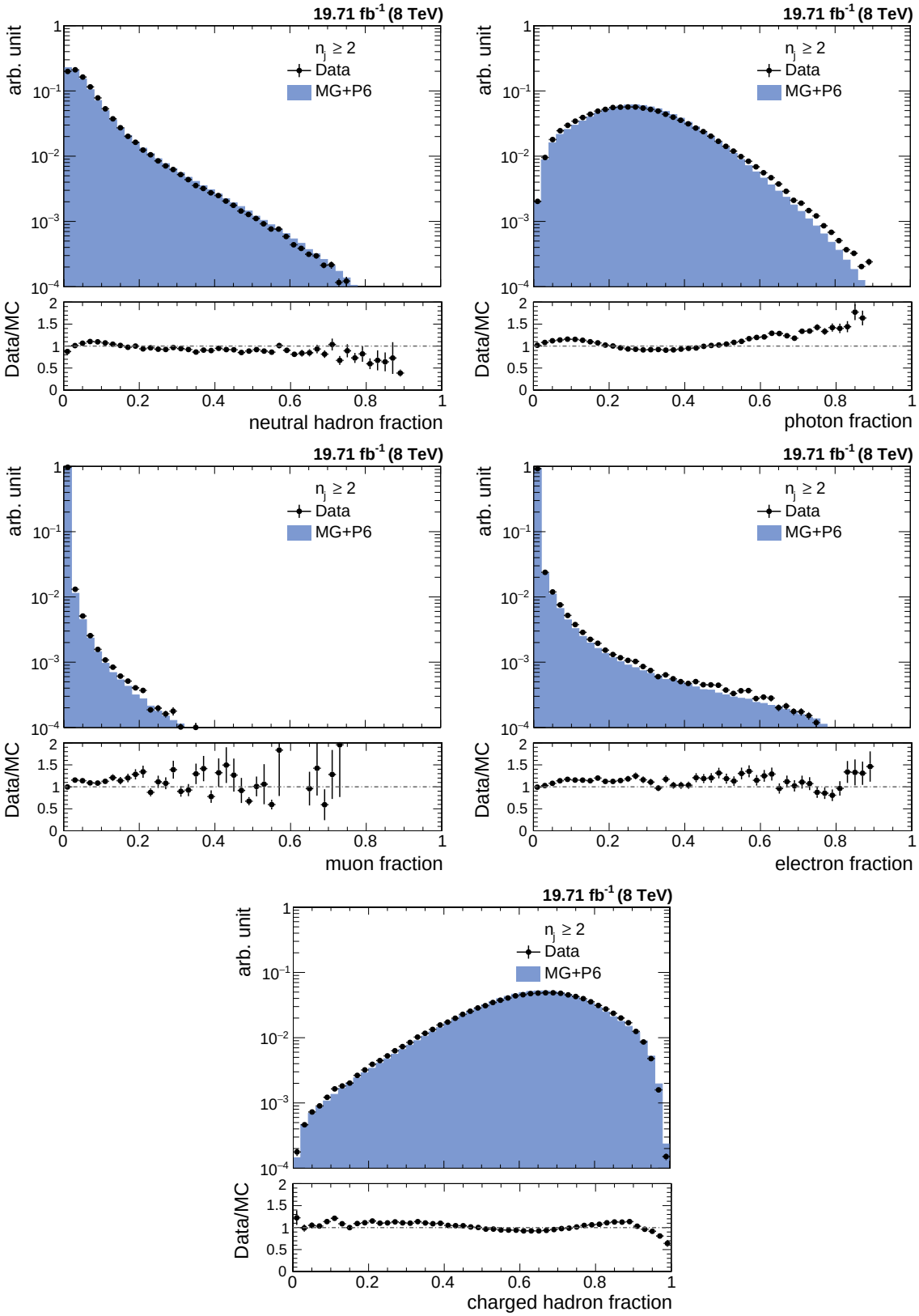

Figure 1.3: The fractions of jet constituents as observed in data and simulated events for different types of PF candidates for inclusive 2-jet events. Data and simulation are normalized to the same number of events. The distributions are shown after the application of the jet ID.

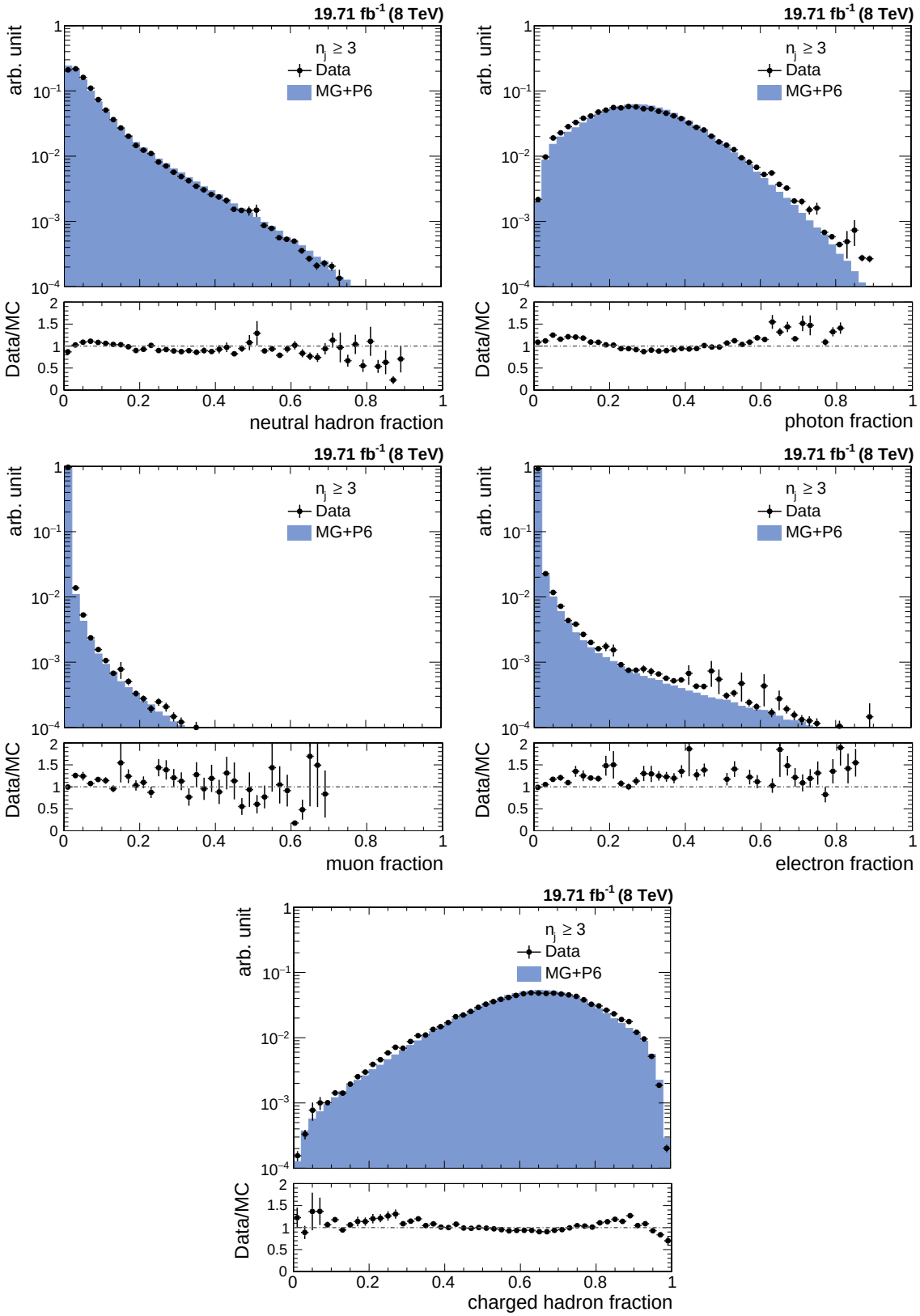

Figure 1.4: The fractions of jet constituents as observed in data and simulated events for different types of PF candidates for inclusive 3-jet events. Data and simulation are normalized to the same number of events. The distributions are shown after the application of the jet ID.

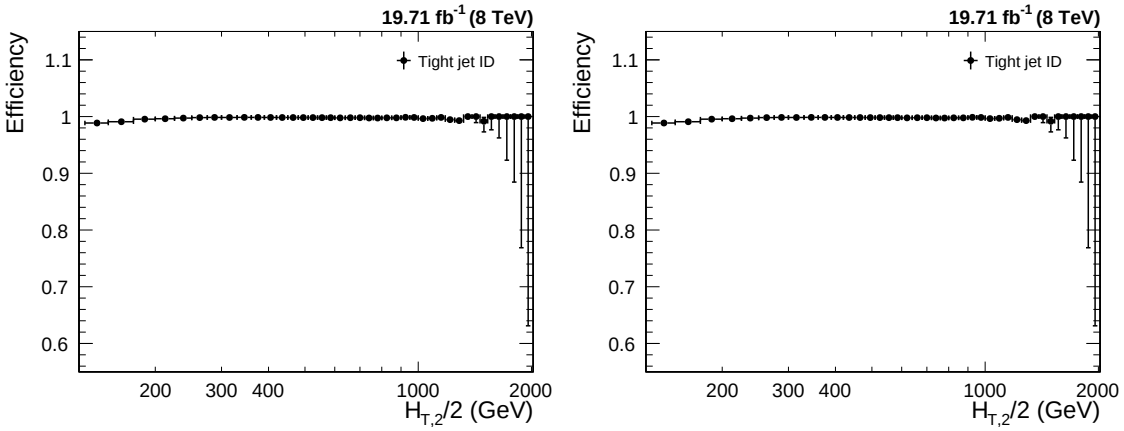

Figure 1.5: The jet ID efficiency studied using a tag-and-probe technique on dijet event topologies, is shown as a function of $H_{T,2}/2$ for inclusive 2-jet (left) and 3-jet events (right) and it always exceeds 99%.

1.2.5 Jet Energy Corrections and Selection

The measurement presented in this thesis is based on jets clustered from PF candidates using the anti-k$_t$ jet algorithm with a size parameter of 0.7. All the jet energy corrections, described in section ? and recommended by CMS, are applied prior to this selection in order to have the correct energy scale of the jets. These comprises different correction levels for jets in data[2] and for jets in simulated events[3]. The jet selection, based on phase space cuts on transverse momentum and rapidity of jets in an event, is as follows :

- All jets having $p_T > 150$ GeV and $|y| < 5.0$ are selected.
- Events with at least two jets are selected.
- The two leading jets should have $|y| < 2.5$ and further jets are counted only, if they lie within the same central rapidity range of $|y| < 2.5$.

These cuts assure high detector acceptance and exactly same selection is applied in the measurement, simulated events as well in theoretical calculations for a consistent

[2]The JEC version applied on data is internally referred to as Winter14_V8
[3]The latest JEC for run-independent Monte Carlo Samples are called START53_V27

comparison.

1.3 Comparison with Simulated Events

1.3.1 Pile-up Reweighting

The official Monte-Carlo samples are generated with distributions for the number of pileup interactions which is meant to roughly cover, though not exactly match the conditions expected for each data-taking period. To still get comparable pile-up distributions in data and simulated events, the simulated events are reweighted with a weight w_{PU} to match the distribution in data :

$$w_{PU} = \frac{N_{data}(N_{PU}, \text{est.})/\sum N_{data}}{N_{MC}(N_{PU}, \text{truth})/\sum N_{MC}} \tag{1.5}$$

Figure 1.6 shows the number of reconstructed vertices before and after reweighting. The significant mismatch of the pile-up distributions in data and simulated events, which is present before the reweighting, completely vanishes.

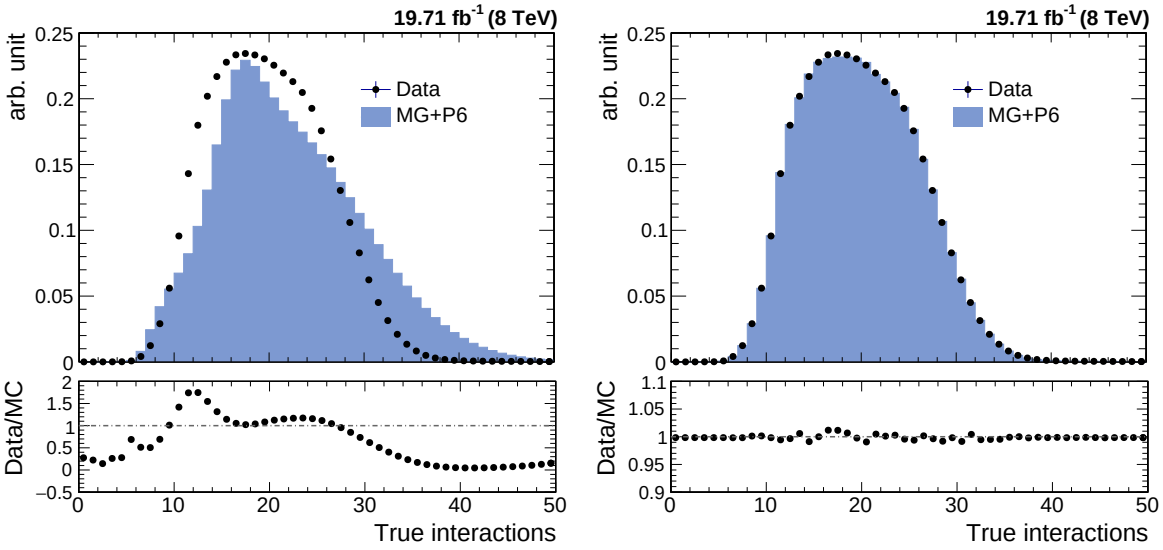

Figure 1.6: Number of reconstructed vertices in data and simulated events before (left) and after (right) the pile-up reweighting.

1.3.2 Cross Section Comparison

The inclusive differential multijet cross sections are measured as a function of the average transverse momentum, $H_{\mathrm{T},2}/2 = \frac{1}{2}(p_{T,1} + p_{T,2})$ where $p_{T,1}$ and $p_{T,2}$ denote the transverse momenta of the two leading jets, and is defined by the basic formula :

$$\frac{\mathrm{d}\sigma}{\mathrm{d}\big(H_{\mathrm{T},2}/2\big)} = \frac{1}{\epsilon\mathcal{L}_{\mathrm{int,eff}}} \frac{N}{\Delta\big(H_{\mathrm{T},2}/2\big)} \tag{1.6}$$

where

- N is the number of jets counted in a bin,
- $\mathcal{L}_{\mathrm{int,eff}}$ is the effective integrated luminosity,
- ϵ is the product of the trigger and jet selection efficiencies (greater than 99%),
- $\Delta\big(H_{\mathrm{T},2}/2\big)$ are the bin widths in $H_{\mathrm{T},2}/2$.

The measurements are reported in units of (pb/ GeV). The inclusive 2-jet events results are represented by $\mathrm{n}_j \geq 2$, inclusive 3-jet events results by $\mathrm{n}_j \geq 3$ and inclusive 4-jet events results by $\mathrm{n}_j \geq 4$ in the figures. The differential cross section is studied for inclusive 2-jet, inclusive 3-jet and inclusive 4-jet events. Then ratio R_{mn} as a function of $H_{\mathrm{T},2}/2$ is studied which is the ratio of the differential cross section of selected inclusive m-jet events to that of inclusive n-jet events in each $H_{\mathrm{T},2}/2$ bin ($\mathrm{m} > \mathrm{n}$ and $\mathrm{m} \neq \mathrm{n}$),

$$R_{mn} = \frac{\left[\frac{\mathrm{d}\sigma}{\mathrm{d}\left(H_{\mathrm{T},2}/2\right)}\right]_{(m\text{-}jet)}}{\left[\frac{\mathrm{d}\sigma}{\mathrm{d}\left(H_{\mathrm{T},2}/2\right)}\right]_{(n\text{-}jet)}} \tag{1.7}$$

In this section we have detector level comparison of differential cross section of 2012 full data with NLO predictions as well as MadGraph5 + pythia6 MC simulations. Figure 1.7 shows the comparison of differential cross section as a function of $H_{T,2}/2$ for inclusive 2-jet events (top left) and inclusive 3-jet events (top right), for data (black solid circles), MadGraph5 + pythia6 MC (red solid circles) and NLO (histogram). At present, for inclusive 4-jet events (bottom), the results from data and MC are available. NLO predictions are yet to be done for this case. Each plot also shows the ratio between the MC predictions and the data as well as between the NLO predictions and the data. Di-jet production is known to suffer from large corrections from soft gluon radiation which requires re-summation beyond fixed order perturbation theory. Theoretical predictions at NLO including the parton shower (NLO+PS) allow to account for these effects and obtain a better description of the available data. 150-200 bins are not included to avoid the infrared sensitivity for the bins next to min. p_T cut in NLO calculations for inclusive 2-jet events.

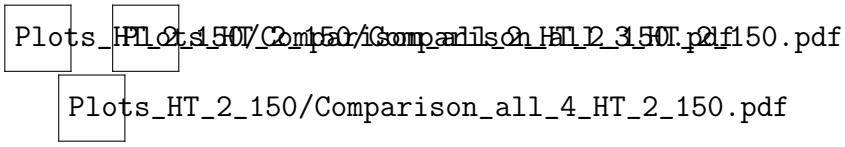

Figure 1.7: The differential cross section as a function $H_{T,2}/2$ for inclusive 2-jet events (top left), for inclusive 3-jet events (top right) and for inclusive 4-jet events (bottom), for data (black solid circles), MadGraph5 + pythia6 MC (red solid circles) and NLO (histogram). Ratios between the MC predictions and the data as well as between the NLO predictions and the data are shown in bottom panel of each plot.

Bibliography

[1] C. Collaboration, "Jet Identification at 8 TeV." https://twiki.cern.ch/twiki/bin/viewauth/CMS/JetID, 2012. (accessed on 2017-10-31).

[2] J. Alwall, M. Herquet, F. Maltoni, O. Mattelaer, and T. Stelzer, "MadGraph 5 : Going Beyond," *JHEP*, vol. 06, p. 128, 2011.

[3] T. Sjostrand, S. Mrenna, and P. Z. Skands, "PYTHIA 6.4 Physics and Manual," *JHEP*, vol. 05, p. 026, 2006.

[4] J. Alwall *et al.*, "A Standard format for Les Houches event files," *Comput. Phys. Commun.*, vol. 176, pp. 300–304, 2007.

[5] C. J. Clopper and E. S. Pearson, "The use of confidence or fiducial limits illustrated in the case of the binomial," *Biometrika*, vol. 26, no. 4, pp. 404–413, 1934.

[6] C. Collaboration, "Jet Performance in pp Collisions at 7 TeV," 2010.

Selected Reprints